Bandlimited raypaths: an example

Marta Jo Woodward

ABSTRACT

SEP–57 proposed projecting traveltimes picked from bandlimited-wavelet peaks back over bandlimited raypaths. These bandlimited raypaths were defined as averages of the imaginary parts of monochromatic, Rytov wavepaths over frequency. This paper relates bandlimited raypaths to the Uncertainty Principle, and provides an example comparing ray and bandlimited-ray inversion. The example illustrates several characteristics of bandlimited raypaths, including their incorporation of wavefront healing and their natural smoothing of inversion.

INTRODUCTION

Ray tomography is based on the assumption of high-frequency data. If traveltimes are to be picked from a wavelet, satisfaction of this assumption requires either that the wavelet peak is undistorted or that a Fermat-path first break can be determined. In practical applications these requirements are rarely met. The velocity field may vary quickly on the scale of the source wavelength (meaning that the wavelet is distorted by geometrical frequency dispersion) and first breaks are hard to pick (owing to overlapping events and low signal level).

SEP–48 introduced the idea of a fat raypath in recognition of the uncertainty inherent in picking bandlimited-wavelet peaks (Woodward, 1986). SEP–57 developed the idea more formally in the context of Rytov diffraction tomography (Woodward, 1988; Rocca and Woodward, 1988; Woodward and Rocca, 1988). With the assumption that a traveltime pick corresponds to an average phase delay, a fat or bandlimited raypath was defined as an average of the imaginary parts of monochromatic, Rytov wavepaths over frequency.

This paper provides an example comparing ray and bandlimited-ray inversion, using time picks from a VSP data set. The first section compares ray and bandlimited-ray backprojection patterns, the second their resulting velocity inversions.

BACKPROJECTION PATTERNS

The data used for this example was drawn from a 9-component data set, with four surface-source locations (roughly in line) and a single receiver moved up and down a 1250-meter well. Only first-arrival, p-wave events were considered, as picked from the vertical-source, vertical-receiver component.

Because the geology in the area was known to be flat, the background velocity model was chosen to increase linearly with depth (v(z)=1450+1.05z, in m/s). Regular and bandlimited raypaths through the model are shown for one shot-geophone pair in the upper two panels of Figure 1. The fat raypath is 2.5-dimensional. It was formed by numerically integrating 3-dimensional, monochromatic wavepaths from 10 to 50 Hz, and then by numerically integrating these patterns over the out-of-the-page dimension. The free surface was ignored. (While the fat raypath is cut off at the well in the figure, the full pattern was used in the inversion below.)

The bottom left-hand panel shows a slice through the full, 3-dimensional, bandlimited raypath. This panel is included to illustrate the zero that appears down the middle of any imaginary, Rytov, three-dimensional wavepath. The zero is easily explained by a scattering argument: a scatterer in line with the Fermat path generates energy in phase with the background wavefield, affecting only the amplitude.

The bottom right-hand panel in Figure 1 shows a 2.5-dimensional, 10 to 30 Hz wavepath, which is considerably broader than its 10 to 50 Hz equivalent. The width of a bandlimited raypath was calculated in Rocca and Woodward (1988), using the stationary-phase approximation. It was shown to be inversely proportional to the bandwidth over which the monochromatic wavepaths are summed, and independent of the average frequency. The inverse relation between width and bandwidth is perhaps most easily remembered as an example of the Uncertainty Principle: that the bandwidth-duration product of a signal is bounded from below, that

$$\Delta t \Delta \omega \geq 2\pi. \tag{1}$$

Δt corresponds to the time window of the trace examined (i.e., for traveltime picks, the sample rate). Since it dictates the averaging of frequency information in the Fourier domain, it is inversely proportional to the bandwidth of the applicable fat raypath. Because it also limits the distance detectable scatterers can stray from the Fermat path, it is directly proportional to the fat raypath's width.

The top two panels in Figure 2 show the composite coverage of regular and bandlimited raypaths for the full data set (268 shot-geophone pairs). The panels differ not only in the area covered, but also in the weighting of the area covered. Because the fat raypaths take scattering into account, they are high in amplitude at the source and receiver and low in amplitude elsewhere. This weighting is an expression of wavefront healing.

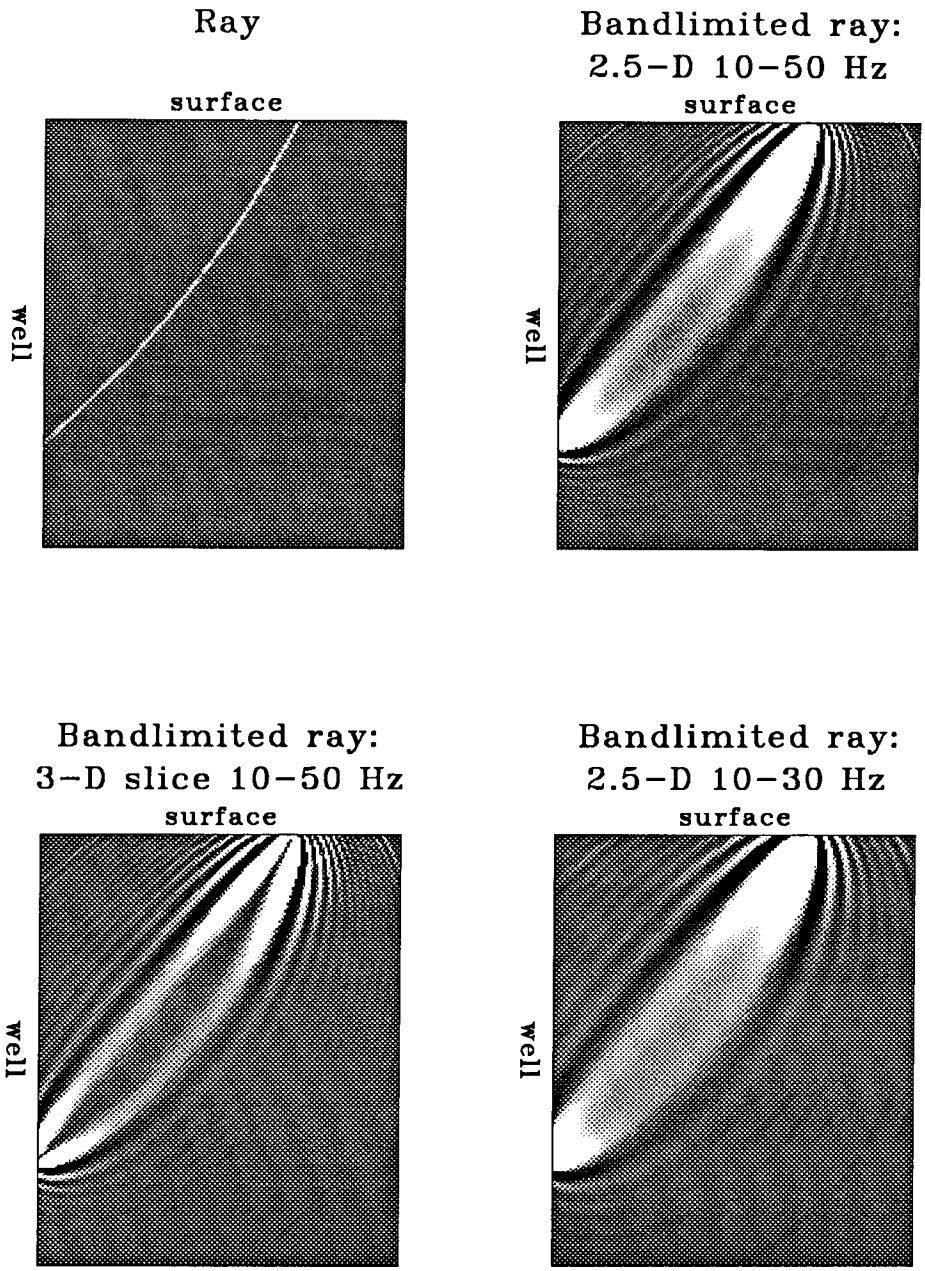

FIG. 1. Backprojection patterns. From left to right, top to bottom: a raypath; a 2.5-D, 10-50 Hz bandlimited raypath; a slice through a 3-D, 10-50 Hz bandlimited raypath; a 2.5-D, 10-30 Hz raypath. The first panel is unclipped (pclip=100); the last three panels clip 5% of the data points (pclip=95).

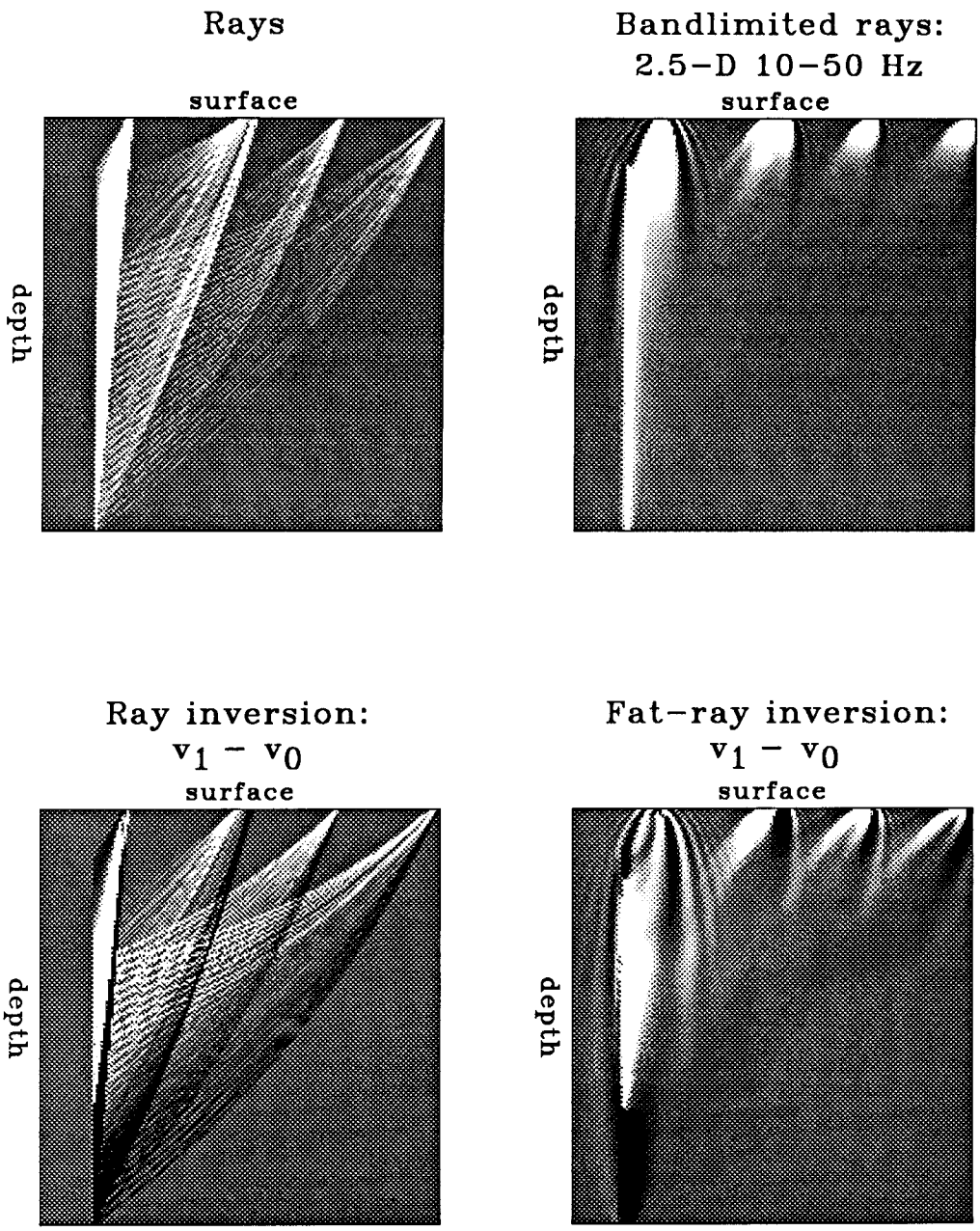

FIG. 2. Velocity inversions. From left to right, top to bottom: the total ray coverage; the total fat-ray coverage; perturbations to the background velocity field after one linear step of ray inversion ($v_1 - v_0$); perturbations to the background velocity field after one linear step of fat-ray inversion ($v_1 - v_0$). The panels all clip 5% of their data (pclip=95).

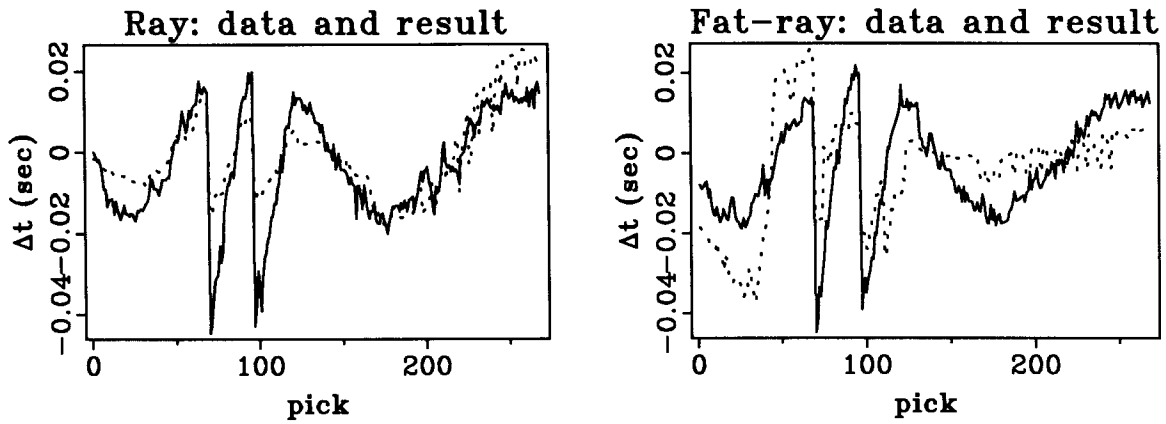

FIG. 3. Traveltime data. The solid curves show the picked time-delay data; the dotted curves show the delays calculated by ray and fat-ray forward modelling through the inversion results.

INVERSIONS

The bottom two panels in Figure 2 compare the ray and fat-ray velocity inversions achieved after one linear step. The results are plotted as perturbations to the background velocity field, $v_1 - v_0$. For the ray inversion, first-break traveltimes were projected back over raypaths; for the fat-ray inversion, first-peak traveltimes were projected back over bandlimited (10 to 50 Hz) raypaths. Both inversions indicate low-velocity zones (with respect to the background model) at the top and bottom of the section and a high-velocity zone in the middle. The bandlimited inversion is noticeably smoother than the ray inversion, and it incorporates geometrical-spreading effects. Because the problem was severely underdetermined, the inversions do not look substantially different from the coverage plots in the upper two panels.

The solid curves in the left and right panels of Figure 3 show the traveltime delays used as data in the ray and fat-ray inversions. The dotted curves show delays calculated by ray and fat-ray forward modelling through the inversion results. The picks along the horizontal axes sequentially plot the source-receiver experiments from shallowest to deepest for the 4 sources. The first 69 picks correspond to the second source from the well; the next 27, 27 and 145 to the fourth, third and first sources from the well (see Figure 2). Clearly, the fat rays have failed to describe the time delays for the source closest to the well, indicating some inconsistency between the model and the data. The inconsistency could result from: errors in the positioning of the source—which are proportionately larger for the source closest to the receivers; errors in the calculation of the fat raypaths; inadequacies in the fat-ray model (i.e., the time pick does not correspond to an average time delay).

CONCLUSIONS

Given the clean first breaks and flat controlling geology of this data set, the assumptions of ray tomography are probably more or less satisfied. Although the problem is severely underdetermined, the ray-tomographic inversion provides a reasonable velocity update and adequately explains the data. The bandlimited-ray inversion yields a velocity update similar to the ray result—but naturally smoothed and more heavily weighted at the source and receiver locations. The smoothing and weighting demonstrate the method's recognition of signal bandwidth and wavefront healing. The failure of the bandlimited rays to explain the traveltime delays for the source closest to the well requires further investigation.

ACKNOWLEDGEMENTS

I thank ARCO for the VSP data set. I also thank Henry Brysk for pointing out that fat rays are an expression of the Uncertainty Principle at Fallen Leaf Lake in 1986.

REFERENCES

Rocca, F., and Woodward, M. J., 1988, Wave-equation tomography–II: SEP–**57**, 25–47.

Woodward, M. J., 1986, Iterative tomography: error projection along ellipses and lines: SEP–**48**, 35–43.

Woodward, M. J., 1988, Wave-equation tomography–I: SEP–**57**, 1–23.

Woodward, M. J., and Rocca, F., 1988, Wave-equation tomography: 58th Ann. Internat. Mtg., Soc. Explor. Geophys., Expanded Abstracts, 1232–1235; available as an SEG slide set.